RESEARCH ARTICLE | MAY 16 2022

Active polar flock with birth and death

Pawan Kumar Mishra ; Shradha Mishra

Physics of Fluids 34, 057110 (2022)
https://doi.org/10.1063/5.0086952

Physics of Fluids ARTICLE scitation.org/journal/phf

Active polar flock with birth and death

Cite as: Phys. Fluids **34**, 057110 (2022); doi: 10.1063/5.0086952
Submitted: 31 January 2022 · Accepted: 2 May 2022 ·
Published Online: 16 May 2022

View Online Export Citation CrossMark

Pawan Kumar Mishra[a] and Shradha Mishra

AFFILIATIONS

Department of Physics, Indian Institute of Technology (BHU), Varanasi, Uttar Pradesh 221005, India

[a]Author to whom correspondence should be addressed: pawankumarmishra.rs.phy19@itbhu.ac.in

ABSTRACT

We study a collection of self-propelled polar particles on a two-dimensional substrate with birth and death. We introduce a minimal lattice model for the system using active Ising spins, where each particle can have two possible orientations. The activity is modeled as a biased movement of the particle along its direction of orientation. The particles also align with their nearest neighbors using Metropolis Monte Carlo algorithm. The system shows a disorder-to-order transition by tuning the temperature of the system. Additionally, the birth and death of the particles is introduced through a birth and death parameter γ. The system is studied near the disorder-to-order transition. The nature of disorder-to-order transition shows a crossover from the first order, discontinuous to continuous type as we tune γ from zero to finite values. We also write the effective free energy of the local order parameter using perturbative calculation, and it confirms the dependence of the nature of phase transition on the birth and death parameter.

I. INTRODUCTION

The active matter systems can be recognized as a collection of particles in which the individual components possess nonzero motility by converting the energy from their surroundings and also from the medium.[1–6] The active particles spontaneously self-organize when present in large numbers and result in coordinated and collective behavior (CB) on various length scales.[4,5,7–13] The phenomenon of collective behavior is being studied with great interest in systems exhibiting nonequilibrium phase transition under driven noise and particle density.[2,14–18] In different experimental,[19–23] analytical,[1–3,24] and numerical[16–18,25–37] studies of active matter systems, it has been shown that the system changes its static and dynamic behavior in different homogeneous and inhomogeneous environments and on the variation of different parameters.[4,38–49] Among them, the nature of phase transition is one of the most studied phenomena in this field of research.[14,16–18,38,50–52] The phase transition in the collection of self-propelled particles also called as "flocking transition" is important because it can be described as a nonequilibrium analog of disorder-to-order phase transition in equilibrium systems.[50–53]

In a recent study of lattice-based models introduced by Peruani *et al.*[50] and Solon and Tailleur,[51] it has been found that the nature of phase transition in self-propelling agents is analogous to the liquid–gas transition on the variation of temperature and density in the system.[51,52] To understand the phase transition, Solon *et al.* introduced a microscopic lattice model with discrete symmetry, which is known as the active Ising model (AIM).[51] The AIM is a much simplified model for the collective motion and gives the basic features of the flocking models:[52] viz., band formation, large density fluctuations, discontinuous disorder-to-order phase transition, etc. The study of AIM by[51] is for the system where the total number of agents is fixed. The effect of birth and death of agents on the system is not yet explored.

In this current study, we ask the question: whether the introduction of birth and death of the agents can affect the nature of phase transition? To serve this purpose, we introduced a minimal lattice-based model of active Ising spins (AIM) with an additional birth and death term γ.

The system is studied for various γ, and it is found that for the $\gamma = 0$, the system shows a first-order, disorder-to-order phase transition with the appearance of bands in the local density and magnetization. On introducing the γ, the bands start to dilute and, finally, disappear for large γ, and the transition becomes continuous in nature. We also studied the system using coarse-grained hydrodynamic equations of motion. Using the renormalized mean-field theory, we write effective free energy for local order parameter and find an additional cubic order nonlinearity present for zero birth and death, and the nonlinearity weakens on increasing birth and death parameter.

The rest of the paper is organized as follows. In Sec. II, we discuss the model and simulation details. In Sec. III, the results from the numerical simulations are discussed where we mainly conclude how the nature of phase transition is changing by tuning the parameter γ. In addition to the numerical approach, we also study the system analytically in Sec. IV with the help of coarse-grained hydrodynamic

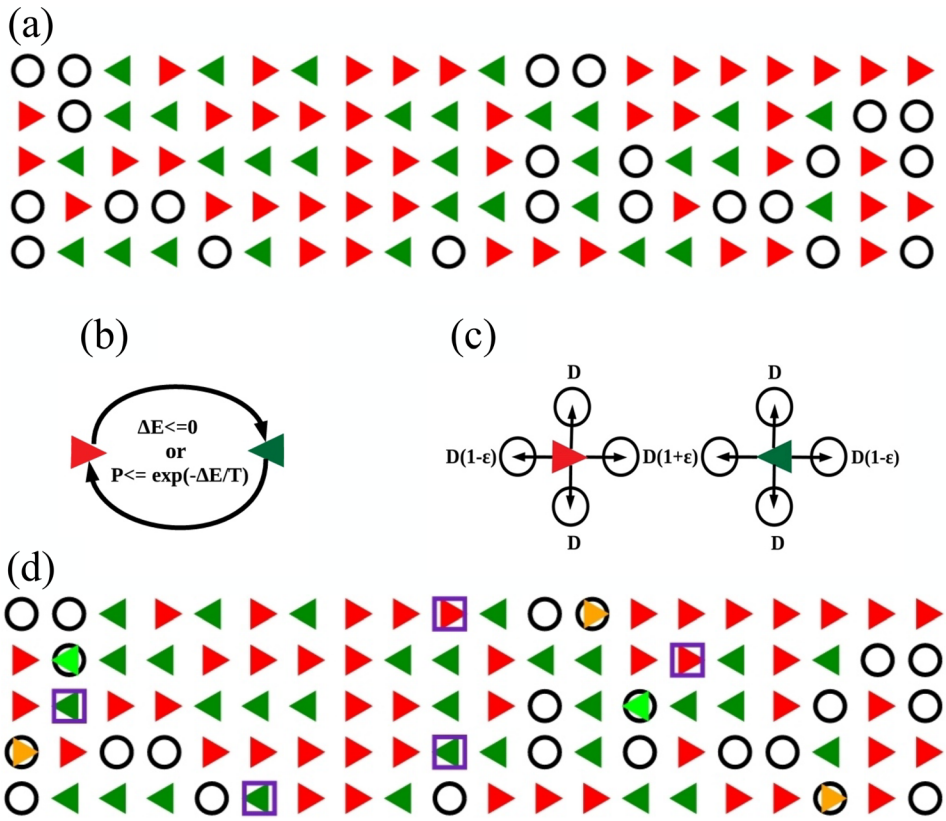

FIG. 1. (a) Sketch of a part of system carrying spins $S = +1$ [red (triangle right)] and $S = -1$ [dark green (triangle left)] along with vacant sites $S = 0$ (black circle) on a two-dimensional lattice, (b) represents the flipping rate at fixed temperature, (c) represents the probability of movement of the spins to the neighboring sites, and in (d), the birth and death parameter γ is added in the model in which the particles disappearing from random sites are shown by magenta square and appearing at the sites which were vacant represented by the orange triangle right for $S = +1$ and the green triangle left for $S = -1$.

equations for density and polarization using the renormalized mean-field theory. Finally, in Sec. V, we conclude the paper with a summary and discussion of the results.

II. MODEL AND NUMERICAL METHODOLOGY

We consider a system of active Ising spins (AIM) on a two-dimensional rectangular lattice of size $L_x \times L_y$ with a periodic boundary condition in both directions. A fraction of sites on the lattice is vacant. Each spin can take two possible values $S_i = \pm 1$. Since some of the sites are vacant, we define an occupancy variable $n_i = 0$ or 1 for the unoccupied and occupied sites, respectively. In this model, the volume exclusion principle is effective such that each site can have a maximum of one particle on it.[50] Each spin can interact with its nearest neighbor spins using the Ising Hamiltonian[55]

$$H = -\sum_{i=1}^{N} n_i n_j S_i S_j, \tag{1}$$

thus, the interaction term is nonzero only if the site and the interacting sites both are occupied. The above Hamiltonian in Eq. (1) is simulated for a fixed vacancy density $V = 20\%$ (particle density $\rho = 0.8$) by tuning the temperature. The temperature is introduced through the Metropolis Monte Carlo algorithm[56,57] for the alignment interaction among the spins. The ratio of the interaction strength and the Boltzmann constant is chosen as 1. Particles tend to move in the direction of their spin if the lattice site is vacant; otherwise, they do not move. The dynamics of the spins on the lattice can be modeled in the following manner: (i) the spins are fixed to their lattice sites and interact through the Hamiltonian in Eq. (1). In this study, we are defining it as "fixed Ising model" (fIm). (ii) We allowed the spin to diffuse to any of its nearest vacant sites with equal probability. The model is named as the diffusive Ising model (dIm). In Fig. 1, we show the Kolmogorov diagram[54] to check the detail balance condition on dIm. In Fig. 1, a loop of four configurations is shown, that breaks Kolmogorov's criterion, e.g., a clockwise loop gives the total probability $D^2 e^{-4\beta}$, while an anticlockwise loop gives $D^2 e^{-2\beta}$, thus showing that the system does not satisfy detailed balance. The numbers associated with the arrows are the transition rates. Hence, *fIm* satisfies the detail balance condition, but the dIm deviates from it, and this observation is consistent with the model studied in Ref. 50.

(iii) Further, we made the spins active by introducing a biased movement corresponding to their direction as introduced in Refs. 51 and 52. The update rules showing the motion of the spins are shown in Fig. 2(b). Activity is introduced through a parameter $\varepsilon \in (0, 1)$. In the presence of activity ε, the update rule for the movement of the spins at a particular site is given as follows. Each particle hops to its two neighboring sites left and right at rate $D(1 + S\varepsilon)$ provided the target site is vacant. It hops to the other two sites (up and down) with equal probability D. If $\varepsilon = 0$, then, the hopping rates are the same in all the directions and that rate comes out to be $D = 1/4$ and the model reduces to dIm. For nonzero ε, the particle moves in the direction of its orientation at rate $D(1 + \varepsilon)$ and in the opposite direction to its

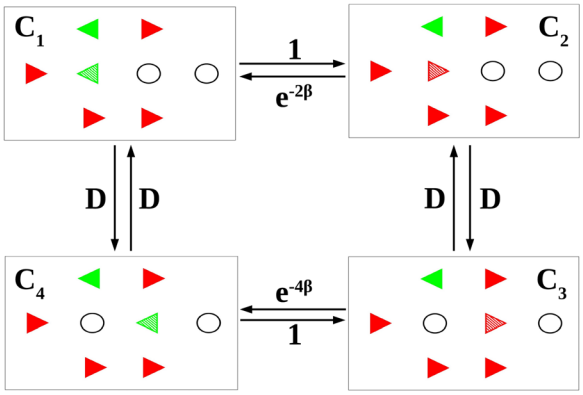

FIG. 2. A loop of four configurations that break Kolmogorov's criterion[54] of detailed balance for dIm, flipping, and movement is shown for the spin represented by partially filled [red (triangle right)] and [dark green (triangle left)]. The clockwise loop ($C_1 \to C_2 \to C_3 \to C_4 \to C_1$) gives the total probability $D^2e^{-4\beta}$, while the anticlockwise loop ($C_1 \to C_4 \to C_3 \to C_2 \to C_1$) gives the total probability $D^2e^{-2\beta}$, thus showing that the system does not satisfy detailed balance. The numbers associated with the arrows are the transition rates, and other symbols have the same meaning as in Fig. 1.

orientation at rate $D(1-\varepsilon)$. Whereas, the particle hops with rate D to the other two possible directions. For our present study, we fix $\varepsilon = 1.0$. We call the model as the active model (Am).

(iv) Next, we introduce the birth and death of particles in the model (Am). The birth and death rate γ is introduced as a fraction of sites on the lattice with particle density ρ, such that from the randomly chosen $\gamma/2$ fraction of sites we remove the particles (if occupied) and similarly on the randomly chosen unoccupied sites, i.e., $\gamma/2$ fraction of the total number of sites, we introduced the new particles with spin favored with the majority spins in their nearest neighbor. We call it the birth and death active model (bdAm), the value of γ is tuned from 0 to 0.1. For $\gamma = 0$, the model reduces to Am. One simulation step is counted after the successful update of the above steps for all the particles once. Total simulation steps (time) used are $T = 1.7 \times 10^5$. The steady-state calculation of various quantities is performed after the simulation time 7×10^4. We use 15 independent realizations for averaging the data for the system sizes $L_x \times L_y = 400 \times 50$, 600×50, and 800×50.

III. RESULTS

We first studied the model (bdAm) with no birth and death rate, i.e., $\gamma = 0$. The system is studied at varying temperatures. A disorder-to-order phase transition is found on decreasing temperature. We studied the system for activity $\varepsilon = 1$ and for different γ. We first calculated the global magnetization in the system defined as

$$M(t) = \frac{1}{N}\left|\sum_i S_i(t)\right|, \tag{2}$$

where N is the total number of particles. We define the mean magnetization $M = \langle M(t)\rangle$, where $\langle\cdot\rangle$ means the average over time in the steady state and over different realizations. We find that for the high temperature and for all γ, the system is disordered ($M \simeq 0$) and ordered with $M \simeq 1$ for the low temperature.

The variation of M as a function temperature is shown in Fig. 3(a) for different γ. We find a very strong dependence on the shape of the disorder-to-order curve on γ. Also, we show the variation of M as a function of temperature for different system sizes $L_x \times L_y = 400 \times 50$, 600×50, and 800×50 for a fixed value of $\gamma = 0.0$, 0.1, and 1.0 in Figs. 3(b)–3(d), respectively. We observe a very insignificant change in the curves with respect to system size, and we expect that the present model has a very weak finite-size effect in comparison to other studies of Vicsek's type models.[14]

To confirm the nature of transition, we looked at the system near the disorder-to-order transition. We first plot the real space snapshot of local density ρ_{loc} in Figs. 4(a)–4(c). The ρ_{loc} is calculated by counting the density of spins in a box of size 2×2. The panels from top to bottom (t_1–t_3) for three different simulation times $t = 1.4 \times 10^5$, 1.5×10^5, and 1.6×10^5, respectively. The panel (a)–(c) is for $\gamma = 0$, 0.01, and 0.1, respectively. For $\gamma = 0$, we see the formation of bands of high-density spins, and with the time, these bands move across the system. The bands get diluted on increasing γ and disappear for large value $\gamma = 0.1$. The color bar shows the value of local density ρ_{loc}. Similarly, we also plot the local magnetization m, obtained by calculating the mean spin in the box of size 2×2 in Figs. 4(d)–4(f) for the same set of parameters as for (a)–(c). The panel (d)–(f) is for $\gamma = 0$, 0.01, and 0.1, respectively. We again find for zero γ, bands of high-ordered region move in the background of the disordered region. The bands get diluted on increasing γ and finally disappear for large $\gamma = 0.1$. The color bar shows the value of local m, and positive and negative m represents the mean local spin $+1$ and -1, respectively. Very clearly, the band splits into thinner and weaker bands on the introduction of γ. The formation of bands we find here for $\gamma = 0$ or Am is a common

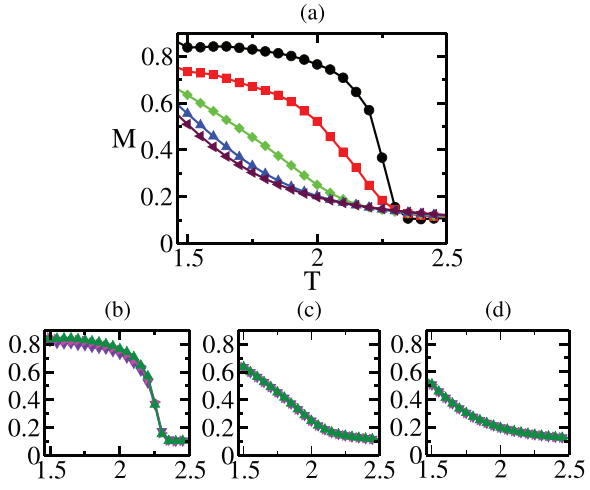

FIG. 3. The plot of order parameter M vs temperature T (a) for the system size 800×50 and various values of γ, i.e., the black (circle), red (square), green (diamond), blue (triangle right), and maroon (triangle left) for $\gamma = 0$, $\gamma = 0.01$, $\gamma = 0.1$, $\gamma = 0.5$, and $\gamma = 1$, respectively. The panels (b), (c), and (d) represent M vs T for fixed $\gamma = 0$, $\gamma = 0.1$, and $\gamma = 1$, respectively. The different curves in each panel (b)–(d) represent different system sizes, i.e., the indigo (triangle down), magenta (triangle right), and green (triangle right) for 400×50, 600×50, and 800×50. The lines are guide to the eyes.

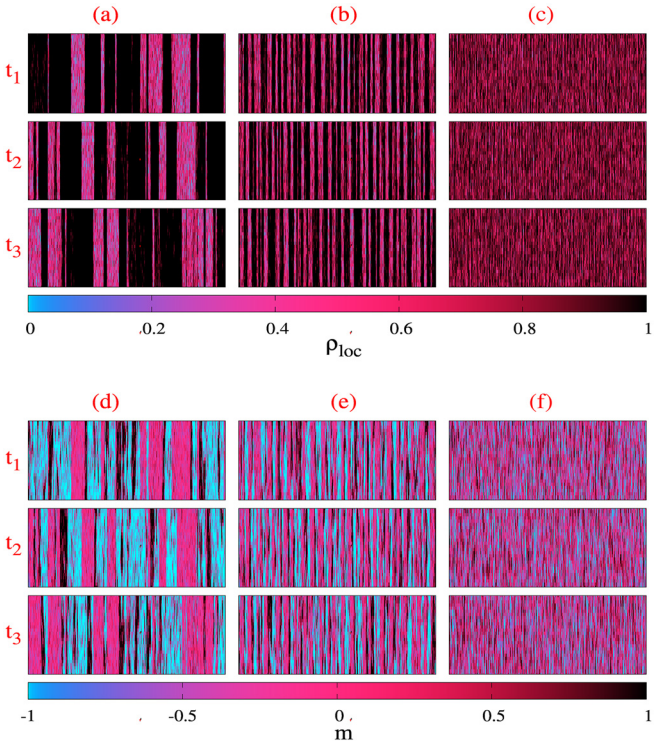

FIG. 4. Time snapshots of local density ρ_{loc} (a)–(c) and local magnetization m (d)–(f). From left to right (a)–(c) or (d)–(f) is for $\gamma = 0.0$, 0.01, and 0.1 and (t_1–t_3) is for 1.4×10^5, 1.5×10^5, 1.6×10^5, respectively. Color bars represent the value of the local density ρ_{loc} and magnetization m. System size is 400×50, and only a part of the system is shown for better resolution.

characteristic of a polar flock.[14,50–52,58] For large $\gamma \simeq 0.1$, slowly, the density pattern disappears and it's all become close to the mean density $\rho_{loc} = 0.8$.

To further characterize the density inhomogeneity for different γ, we plot the distribution of density for different temperatures close to disorder-to-order transition. Using the local density ρ_{loc} plots shown in Figs. 4(a)–4(c), we calculated the local density along the long axis of the system by averaging over the shorter axis L_y. In this manner, we find the density variation in one direction ρ_x. We further plot the probability distribution function (PDF) of density $P(\rho_x)$ for various γ in Fig. 5. For zero γ, distribution clearly shows the bimodal nature, with one peak close to 1 (maximum density) and another peak at the lower density $\rho_x = 0.4$. As we increase γ, the two peaks come closer, and finally, for $\gamma \geq 0.1$, we find a single peak at $\rho_x = 0.8$. In inset of Fig. 5, we plot the density difference of two peaks $\Delta\rho$ vs γ, and plot clearly shows a monotonic decrease of $\Delta\rho$ on increasing γ.

To understand the effect of γ on the nature of phase transition in the system, we observed the time series of the global magnetization $M(t)$ in the steady state for two different $\gamma = 0$ and $\gamma = 0.1$. Using the time series, we calculated the probability distribution function (PDF) of magnetization $P(M)$. In Fig. 6, we plot the $P(M)$ in the vicinity of disorder-to-order transition. Figures 6(a) and 6(b) show the $P(M)$ for $\gamma = 0$ and $\gamma = 0.1$, respectively. Figure 6(a) shows a bimodal distribution of $P(M)$ with one peak at $M = 0.05$ and another at $M = 0.45$ for some intermediate temperature $T = 2.25$ and in the neighborhood of

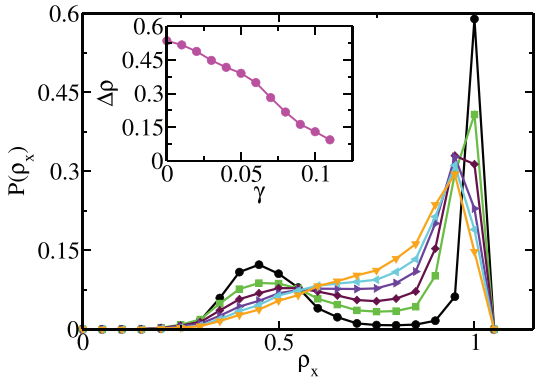

FIG. 5. Plot of PDF $P(\rho_x)$ for different values of γ, i.e., the black (circle), green (square), maroon (diamond), indigo (triangle right), cyan (triangle left), and orange (triangle down) symbols represent $\gamma = 0$, $\gamma = 0.02$, $\gamma = 0.04$, $\gamma = 0.06$, $\gamma = 0.08$, and $\gamma = 0.1$, respectively. The lines are guide to eyes. Inset: plot of $\Delta\rho$ vs γ, where $\Delta\rho$ represents the difference between two peaks of the distribution of the local density. The system size is same as in Fig. 4.

$T = 2.25$, $T = 2.15, 2.20, 2.30, 2.35$, we find jump in the peak position of $P(M)$. Whereas, the distribution is always unimodal for all T, and the location of peak in $P(M)$ smoothly moves toward lower M values for $\gamma = 0.1$ as shown in Fig. 6(b). Hence, we say that the nature of the phase transition changes from the discontinuous to continuous type on increasing γ. In this paper, we mainly focused on the effect of birth and death (bdAm). We also performed the study for zero birth and death and varying the activity $\varepsilon \in (0, 1)$. We found that the nature of phase transition and the behavior of magnetization vs temperature curves changes from continuous to discontinuous type on varying ε (data not shown). These findings are consistent with the study of Peruani *et al.*[50]

Now, using coarse-grained hydrodynamic equations of motion, we show how the increasing birth and death parameter in the density equation can lead to continuous transition.

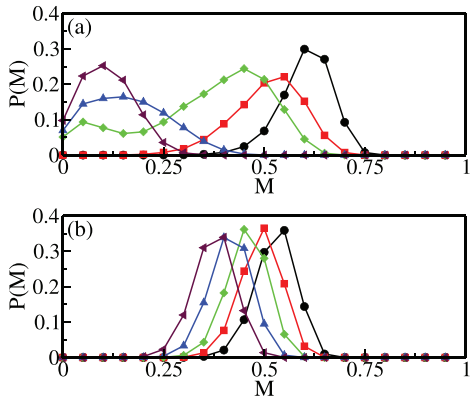

FIG. 6. Plot of PDF of order parameter $P(M)$ for $\gamma = 0$ and $\gamma = 0.1$ in (a) and (b), respectively, where the black (circle), red (square), green (diamond), blue (triangle left), and maroon (triangle up) symbols represent the temperatures: (a) $T = 2.15$, $T = 2.20$, $T = 2.25$, $T = 2.30$, and $T = 2.35$, respectively and (b) $T = 1.65$, $T = 1.70$, $T = 1.75$, $T = 1.80$, and $T = 1.85$, respectively, near the disorder-to-order transition. Lines are guide to eyes. The system size is same as in Fig. 4.

IV. HYDRODYNAMIC EQUATIONS OF MOTION FOR SLOW VARIABLES

Now, we introduce the coarse-grained hydrodynamic equations of motion for slow variables: density $\rho(\mathbf{r},t)$ and polarization order parameter $\mathbf{P}(\mathbf{r},t)$. The former is globally conserved, and the latter is nonzero for the broken symmetry or ordered state. The equation of motion for local density field $\rho(\mathbf{r},t)$

$$\frac{\partial\rho}{\partial t} = -v_0\nabla\cdot(\mathbf{P}\rho) + D_\rho\nabla^2\rho + \gamma g(\rho), \tag{3}$$

and the hydrodynamic equation of motion for the local polarization $\mathbf{P}(\mathbf{r},t)$

$$\frac{\partial\mathbf{P}}{\partial t} = (\alpha_1(\rho) - \alpha_2|\mathbf{P}|^2)\mathbf{P} - v_1\nabla\rho + \lambda(\mathbf{P}\cdot\nabla\mathbf{P}) + D\nabla^2\mathbf{P}. \tag{4}$$

Equation (3) represents a continuity equation with the additional birth and death term $g(\rho) = \rho(\rho_0 - \rho)$ for the density field ρ, where ρ_0 is the mean density of particles in the system and γ is the birth and death parameter. This type of term was first put by Malthus,[59] and consequently, the flocks with birth and death are also known as Malthusian flocks. According to Malthus, any collection of entities that is reproducing and dying can only reach a nonzero steady state with the population density ρ_0. $g(\rho)$ increases with increasing ρ for $\rho < \rho_0$, and it decreases with increasing ρ for $\rho > \rho_0$. The first term on the right-hand side of Eq. (3) describes the convection due to the self-propulsion velocity $v_0\mathbf{P}$. The second term on the right-hand side of Eq. (3) is diffusion due to the density gradient. In polarization $\mathbf{P}(\mathbf{r},t)$, Eq. (4), the first term on right-hand side represents a mean-field transition from an isotropic state ($\mathbf{P} = 0$) to a broken symmetry state $\mathbf{P} = \sqrt{\frac{\alpha_1(\rho_0)}{\alpha_2}}\hat{\mathbf{x}}$ (the direction of broken symmetry is chosen the along x- axis). The second and third terms indicate the hydrostatic pressure due to the density gradient and convection in the model, respectively. Both λ and v_1 depend on the self-propelled speed of the particle.[60] The fourth term represents diffusion in the polarization field. The above two equations are similar to the equations introduced in Ref. 3. Here, we introduced an additional term due to birth and death in the density equation.

We first find the mean-field homogeneous ordered steady state of Eqs. (3) and (4), $\rho = \rho_0$ and $\mathbf{P} = P_0 = \sqrt{\frac{\alpha_1(\rho_0)}{\alpha_2}}\hat{\mathbf{x}}$. We further add a small perturbation on the above homogeneous ordered state and write $\rho(\mathbf{r},t) = \rho_0 + \delta\rho(\mathbf{r},t)$ and $\mathbf{P}(\mathbf{r},t) = (P_0 + \delta P_x)\hat{x} + \delta P_y\hat{y}$. The perturbations $\delta\rho(\mathbf{r},t)$, $\delta P_x(\mathbf{r},t)$, and $\delta P_y(\mathbf{r},t)$ are the small fluctuations in the density and two components of polarization, respectively. Since the system shows a mean-field transition from disordered-to-ordered state where α_1, changes sign. We assumed that the system is close to the critical point such that the order parameter is small, and hence, we have calculated the model for $\alpha_1 = 0$ (at the mean-field critical point). The change in the critical point goes beyond the mean-field study in another interesting research problem and explored in other previous studies of active systems.[61] We further substitute for the ρ and $\mathbf{P}$ from the above expressions and write the Eqs. (3) and (4) for the small fluctuations $\delta\rho, \delta P_x$, and δP_y to the linear order. The equation for δP_x will not contribute to linear order. Hence, only the equations for the local density fluctuation $\delta\rho(\mathbf{r},t)$ and local transverse polarization fluctuation $\delta P_y(\mathbf{r},t)$ will survive.

$$\partial_t\delta\rho(r,t) = -v_0\partial_y\delta P_y - \gamma\rho_0\delta\rho + D_\rho\nabla^2\delta\rho, \tag{5}$$

$$\partial_t\delta P_y = -\partial_y\frac{v_1}{2\rho_0}\delta\rho + D\nabla^2\delta P. \tag{6}$$

We further take the Fourier transform of the two equations using $\hat{\mathbf{A}}(\mathbf{q},\omega) = \int\mathbf{A}(\mathbf{r},t)\exp(i\mathbf{q}\cdot\mathbf{r} + i\omega t)d\mathbf{r}dt$, where $\hat{\mathbf{A}} = (\delta\hat{\rho}, \delta\hat{P}_y)$. We use the method of Fourier transform to solve the modes of the coupled nonlinear partial differential equations of motion for the density and polarization in Eqs. (3) and (4). A similar approach is used earlier in the system of the polar flock as well as in fluid mechanics in Refs. 3 and 62. Applying the Fourier transform, the two equations will become

$$(-i\omega + D_\rho q^2 + \gamma\rho_0)\delta\rho + iq_y v_0\rho_0\delta P_y = 0 \tag{7}$$

and

$$iq_y\frac{v_1}{2\rho_0}\delta\rho + (-i\omega + Dq^2)\delta P_y = 0. \tag{8}$$

The fields $(\delta\rho, \delta P_y)$ in Eqs. (7) and (8) and later equations are in the Fourier transform, but the $\hat{}$ symbol is removed for simplicity. The wavevector $\mathbf{q} = (q\cos(\theta), q\sin(\theta)) = (q_x, q_y)$, where θ is the angle from the direction of broken symmetry.

We further solve the above two coupled linear equations for $\delta\rho$ and δP_y (7) and (8), respectively, and find the solution for the two modes $\omega_\pm$ as

$$\omega_\pm = \frac{-i\gamma\rho_0}{2} \pm \frac{q}{2}\sqrt{2v_0v_1 + 2\gamma\rho_0(D_\rho - D)}. \tag{9}$$

The first term in the two modes shows the exponential decay of the two fields (density and polarization) due to the nonzero birth and death $\gamma \neq 0$ that represents the decay of the traveling mode for finite birth and death. The second term is like sound mode, with speed proportional to the system parameters (self-propulsion speed of the particles and two diffusion constants).

In Sec. IV A, we carry out the perturbative study of the hydrodynamic equations of motion to the lowest (quadratic) order nonlinearity. The aim of the perturbative study is to solve the coupled equations for the density and write an effective equation for the polarization. The effective polarization equation is renormalized, and hence, we name the method as the renormalized mean-field study.

A. Perturbative calculation for effective free energy for local polarization

We focus our study near the disorder-to-ordered critical point and aim to write an effective renormalized equation for polarization after solving for density. To do so, we assume the polarization fluctuation is small and perform the study around the isotropic or disordered state as in the usual Landau–Ginzburg approach.[63]

We introduce $\rho = \rho_0 + \delta\rho$ and $\mathbf{P} = (\delta P_x, \delta P_y)$ and write the equations for the small fluctuations $\delta\rho$ and $\delta\mathbf{P} = (\delta P_x, \delta P_y)$. The solution for the Fourier transformed local density fluctuation $\delta\rho(\mathbf{q},\omega)$ and polarization fluctuations $\delta\mathbf{P}(\mathbf{q},\omega)$ will become

$$\delta\rho(\mathbf{q},\omega) = \frac{-v_0\rho_0 i\mathbf{q}.\delta\mathbf{P}(\mathbf{q},\omega)}{(-i\omega + D_\rho q^2 + \gamma\rho_0)} - \frac{1}{2}\frac{v_0 i\mathbf{q}.\int[\delta P(\mathbf{k},\Omega)\delta\rho(\mathbf{q}-\mathbf{k},\omega-\Omega) + \delta P(\mathbf{q}-\mathbf{k},\omega-\Omega)\delta\rho(k,\omega)]d\mathbf{k}d\Omega}{(-i\omega + D_\rho q^2 + \gamma\rho_0)} \tag{10}$$

and

$$\begin{aligned}-i\omega\delta\mathbf{P}(\mathbf{q},\omega) = &-\alpha_1(\rho_0)\delta\mathbf{P}(\mathbf{q},\omega) + \alpha_1'(\rho_0)\\ &\times\frac{1}{2}\Big[\int\delta\mathbf{P}(\mathbf{k},\Omega)\delta\rho(\mathbf{q}-\mathbf{k},\omega-\Omega)\\ &+\delta\mathbf{P}(\mathbf{q}-\mathbf{k},\omega-\Omega)\delta\rho(\mathbf{k},\Omega)d\mathbf{k}d\Omega\Big]\\ &-\alpha_2\int\delta\mathbf{P}(\mathbf{k},\Omega)\delta\mathbf{P}(\mathbf{k}',\Omega-\Omega')\\ &\times\delta\mathbf{P}(\mathbf{q}-\mathbf{k}-\mathbf{k}',\omega-\Omega-\Omega')d\mathbf{k}d\mathbf{k}'d\Omega d\Omega\,.\end{aligned} \tag{11}$$

Here, we write only the first two terms in the polarization Eq. (4). $\alpha_1'(\rho_0) = \frac{\partial\alpha_1}{\partial\rho}|_{\rho=\rho_0}$. Substituting for $\delta\rho$ leading order from Eq. (10) and substituting for one of mode ω_+ from Eq. (9)

$$\begin{aligned}-i\omega\delta\mathbf{P}(\mathbf{q},\omega) = &\alpha_1(\rho_0)\delta\mathbf{P}(\mathbf{q},\omega) + \frac{1}{2}\alpha_1'(\rho_0)\\ &\times\Bigg[\frac{\int(\delta\mathbf{P}(\mathbf{k})(v_0\rho_0(\mathbf{q}-\mathbf{k}))\delta\mathbf{P}(\mathbf{q}-\mathbf{k},\omega-\Omega))}{6\gamma\rho_0 + (q-k)\sqrt{2v_0v_1+\gamma\rho_0(D_\rho-D)}}\\ &+\frac{\int(\delta\mathbf{P}(\mathbf{q}-\mathbf{k},\omega-\Omega)(v_0\rho_0\mathbf{k})\delta\mathbf{P}(\mathbf{k},\Omega))}{\gamma\rho_0 + k\sqrt{2v_0v_1+\gamma\rho_0(D_\rho-D)}}\Bigg]\\ &-\alpha_2\int\delta\mathbf{P}(\mathbf{k},\Omega)\delta\mathbf{P}(\mathbf{k}',\Omega-\Omega')\\ &\times\delta\mathbf{P}(\mathbf{q}-\mathbf{k}-\mathbf{k}',\omega-\Omega-\Omega')d\mathbf{k}d\mathbf{k}'d\Omega d\Omega.\end{aligned} \tag{12}$$

It is complicated to solve the above equation for the dimensions $d=2$ when $\delta\mathbf{P}$ is a vector. However, the usual flocking transition is characterized by the appearance of bands near the transition.[14,16,51] When bands form, the local density and polarization show the variation only along the direction of moving bands, and in the transverse direction, it is homogeneous both in space and in time. Hence, the system can be considered one dimensional where both $\delta\mathbf{P}$ and $\delta\rho$ only vary along the direction of moving bands and all the vectors can be replaced by scalars in Eq. (12). In such conditions, we can rewrite Eq. (12) as

$$\begin{aligned}-i\omega\delta P(\mathbf{q},\omega) = &\alpha_1(\rho_0)\delta P(q,\omega) + \frac{1}{2}\alpha_1'(\rho_0)\\ &\times\Bigg[\frac{v_0\rho_0\int\delta P(q-k,\omega-\Omega)(q-k)\delta P(k,\Omega)dkd\Omega}{6\gamma\rho_0 + (q-k)\sqrt{2v_0v_1+\gamma\rho_0(D_\rho-D)}}\\ &+\frac{v_0\rho_0\int\delta P(q-k,\omega-\Omega)k\delta P(k,\Omega)dkd\Omega}{6\gamma\rho_0 + k\sqrt{2v_0v_1+\gamma\rho_0(D_\rho-D)}}\Bigg]\\ &-\alpha_2\int\delta P(k,\Omega)\delta P(k',\Omega')\\ &\times\delta P(q-k-k',\omega-\Omega-\Omega')dkdk'd\Omega d\Omega'.\end{aligned} \tag{13}$$

Case with no birth and death

For $\gamma=0$ or no birth and death, by doing the inverse Fourier transform, we write the effective free energy $\mathscr{F}_{eff}(\delta P)$ using Eq. (13) as

$$\begin{aligned}\mathscr{F}_{eff}(\delta P) = &-\frac{\alpha_1(\rho_0)}{2}\int d^2r(\delta P(r))^2\\ &-\frac{\alpha_1'(\rho_0)}{6}\sqrt{\frac{v_0}{2v_1}}\int d^2r(\delta P(r))^3 + \alpha_2\frac{1}{4}\int d^2r(\delta P(r))^4.\end{aligned} \tag{14}$$

For homogeneous δP, the effective free energy $\mathscr{F}_{eff}(\delta P)$ which is real space will become

$$\mathscr{F}_{eff}(\delta P) = -\alpha_1(\rho_0)\frac{\delta P^2}{2} - \frac{\alpha_1'(\rho_0)}{6}\sqrt{\frac{v_0}{2v_1}}\delta P^3 + \frac{\alpha_2}{4}\delta P^4. \tag{15}$$

The constants appearing in Eq. (15) due to finite volume integration are absorbed in the coefficients. The second term of the right-hand side of Eq. (15) is an additional expression which is cubic in order $\mathcal{O}(\delta P^3)$. The presence of such a nonlinear term can lead the mean-field transition to the first order.

Case with birth and death

Now, we examine the system for finite γ, using the denominator of Eq. (13) inside the square [·] bracket

$$\gamma\rho_0 \gg \frac{q\sqrt{2v_0v_1+\gamma\rho_0(D_\rho-D)}}{6}. \tag{16}$$

Then, the second term in Eq. (13) is of the form of $(P\nabla P)$, and this term can be compared with the convective nonlinear term of the type $\mathbf{P}\cdot\nabla\mathbf{P}$ in the hydrodynamic Eq. (4).

Hence, for large γ, the birth and death term will dominate and the transition will be of the continuous type as predicted by the mean-field theory, whereas for finite and small γ, such that

$$\gamma\rho_0 \ll \frac{q\sqrt{2v_0v_1+\gamma\rho_0(D_\rho-D)}}{6}, \tag{17}$$

the effective free energy for $\mathscr{F}_{eff}(\delta P)$ will become

$$F_{eff}(\delta P) = -\frac{1}{2}\alpha_1(\rho_0)\delta P^2 - \frac{v_0\rho_0\alpha_1'(\rho_0)\delta P^3}{6\sqrt{2v_0v_1+\gamma\rho_0(D_\rho-D)}} + \frac{\alpha_2}{4}\delta P^4. \tag{18}$$

The wavevector dependence of the additional convective nonlinear term in Eq. (13) goes away, and it contributes an additional $\mathcal{O}(\delta P^3)$ nonlinearity in the effective free energy which will lead the transition to the discontinuous type. Therefore, the discontinuous transition happens through the competition of a length scale and birth and death parameter as given in Eq. (17). As shown in Fig. 4, on increasing birth and death term from $\gamma=0$, the bands start splitting and their size

deceases, and the nature of transition becomes more and more continuous type as predicted by the mean-field theory.

We further analyzed the properties of effective free energy in the presence of additional cubic order nonlinearity. In the simplified notation, the effective free energy in Eq. (18) can be rewritten as

$$\mathscr{F}(\delta P) = -\beta_1 \delta P^2 - \beta_2 \delta P^3 + \beta_3 \delta P^4, \tag{19}$$

where $\beta_1 = \frac{1}{2}\alpha_1(\rho_0)$, $\beta_2 = \frac{v_0\rho_0\alpha_1'(\rho_0)}{6\sqrt{2v_0v_1+\gamma\rho_0(D_\rho - D)}}$, $\beta_3 = \frac{\alpha_2}{4}$. For the transition to be the first order, we impose the coexistence condition, i.e., $\mathscr{F}(\delta P = 0) = \mathscr{F}(\delta P \neq 0)$, that gives

$$-\beta_1 - \beta_2 \delta P + \beta_3 \delta P^2 = 0, \tag{20}$$

also the condition of steady state implies $\frac{\partial \mathscr{F}}{\partial \delta P} = 0$

$$-2\beta_1 - 3\beta_2 \delta P + 4\beta_3 \delta P^2 = 0, \tag{21}$$

using Eq. (20) and (21), the jump in the order parameter P at the transition

$$\delta P = \frac{\beta_2}{2\beta_3}, \tag{22}$$

is always positive, hence, the finite jump. Substituting the value of δP in Eq. (20) and solve for β_1, we $\beta_1 - \frac{\beta_2^2}{4\beta_3} = 0$. We rewrite the above expression and get $\beta_1^c = \frac{\beta_2^2}{4\beta_3}$ again a positive term. We further analyze the jump in the order parameter and transition point by substituting the value β_2 and β_3 in Eq. (22), we get $\delta P = \frac{4v_0\rho_0\alpha_1'(\rho_0)}{3\alpha_2\sqrt{2v_0v_1+\gamma\rho_0\Delta D}}$, where $\Delta D = D_\rho - D$.

Assuming the temperature dependence of α_1 in the mean-field theory $\alpha_1(\rho, T) = \alpha_0(\rho)(T - T^*)$, T^* is point where there is a mean-field type second-order phase transition for large γ. Here, if we define the true critical temperature as T_c, where $\beta_1 = \frac{\beta_2^2}{4\beta_3}$, we get the critical point $\alpha_1^c(\rho, T) = \alpha_0(\rho)(T_c - T^*) = 2\beta_1 > 0$. Hence, we find that $T_c > T^*$ and $T_c = \frac{\beta_2^2}{2\beta_3\alpha_0} + T^*$. After substituting the value of β_2 and β_3, we find $T_c = T^* + \frac{2v_0^2\rho_0^2\alpha_0'^2\rho_0}{9(2v_0v_1+\gamma\rho_0\Delta D)\alpha_2\alpha_0(\rho_0)}$. Hence, in the simplified notation, we can write

$$T_c = T^* + \frac{A}{B+\gamma}, \tag{23}$$

where $A = \frac{4v_0^2\rho_0^2\alpha_0'^2\rho_0}{9\rho_0\Delta D\alpha_2\alpha_0(\rho_0)}$ and $B = \frac{2v_0v_1}{\rho_0\Delta D}$. For large γ, second term in the expression for T_c is negligible and critical point happens at T^*. As we start tuning γ toward lower values, the phase transition shifts toward right as obtained in our numerical study shown in Fig. 3. Also, δP (the jump in order parameter) is almost zero for large γ that means system approaches critical point continuously as found in our numerical study [Fig. 6(b)]. But, as we start decreasing γ, transition happens with a finite jump in order parameter [Fig. 6(a)].

V. DISCUSSION

We studied a system of active Ising spins with birth and death on a two-dimensional substrate with the periodic boundary condition. The system is studied using the Metropolis Monte Carlo method for the interaction among the spins, and the spins perform the biased move along their direction of orientation. The system is studied for the fixed activity and varying birth and death rate γ. It shows a phase transition from disorder-to-order for all γ and fixed activity on varying temperatures from high to low. The transition is of the first order or discontinuous type for the conserved model ($\gamma = 0$) and becomes second-order continuous type for the birth and death model. Also, transition shifts toward higher temperature on decreasing γ. Hence, the presence of birth and death term tunes the disorder-to-order transition to lower the temperature and shows a crossover from the discontinuous to continuous type in the polar flock.

We also performed and compared the hydrodynamic approach developed for the continuum model with the numerical study performed for the lattice system. The results are compared for the local density and polarization, which can be assumed as like a continuum in the steady state. In our analytical study, we find that for zero birth and death rate, the phase transition is of first order with a finite jump in the polarization as given in Eq. (22), whereas as we increase γ, the jump decreases. Hence, we find a crossover from the discontinuous type of transition to the continuous type on increasing γ. Also, the critical temperature shifts toward higher values as birth and death rate γ decreases in Eq. (23) and matches with what is observed in the numerical simulation Fig. 3. Hence, our study shows the effect of birth and death on the nature of the phase transition of the polar flock. The present model is studied for discrete Ising spins with the Globular conserved model[64] for the spin interaction. It is worth to study the system for the non-conserved Kawasaki type[65] of spin interaction as well as for the off-lattice systems.

ACKNOWLEDGMENTS

S.M. thanks J. K. Bhattacharjee for the useful discussion at the start of the project. S.M. also thanks S. Ramaswamy and M. C. Marchetti for introducing the problem a few years back. S.M. and P.K.M. thank PARAM Shivay for the computational facility under the National Supercomputing Mission, Government of India at the Indian Institute of Technology, Varanasi. The computing facility at the Indian Institute of Technology (BHU), Varanasi, is gratefully acknowledged. P.K.M. thanks U.G.C. (India) for research fellowship.

AUTHOR DECLARATIONS

Conflict of Interest

The authors have no conflicts to disclose.

DATA AVAILABILITY

The data that support the findings of this study are available from the corresponding author upon reasonable request.

REFERENCES

[1] J. Toner, Y. Tu, and S. Ramaswamy, "Hydrodynamics and phases of flocks," Ann. Phys. **318**, 170–244 (2005).
[2] J. Toner and Y. Tu, "Long-range order in a two-dimensional dynamical XY model: How birds fly together," Phys. Rev. Lett. **75**, 4326–4329 (1995).
[3] J. Toner and Y. Tu, "Flocks, herds, and schools: A quantitative theory of flocking," Phys. Rev. E **58**, 4828–4858 (1998).
[4] M. C. Marchetti, J. F. Joanny, S. Ramaswamy, T. B. Liverpool, J. Prost, M. Rao, and R. A. Simha, "Hydrodynamics of soft active matter," Rev. Mod. Phys. **85**, 1143–1189 (2013).

[5]C. Bechinger, R. D. Leonardo, H. Löwen, C. Reichhardt, G. Volpe, and G. Volpe, "Active particles in complex and crowded environments," Rev. Mod. Phys. **88**, 045006 (2016).
[6]T. Vicsek and A. Zafeiris, "Hydrodynamics of soft active matter," Phys. Rep. **517**, 71–140 (2012).
[7]G. Gompper, R. G. Winkler, and S. Kale, "The 2020 motile active matter roadmap," J. Phys.: Condens. Matter **32**, 193001 (2020).
[8]D. Saintillan, "Extensional rheology of active suspensions," Phys. Rev. E **81**, 056307 (2010).
[9]T. Shen and P. G. Wolynes, "Stability and dynamics of crystals and glasses of motorized particles," Proc. Natl. Acad. Sci. **101**, 8547–8550 (2004).
[10]C. Dombrowski, L. Cisneros, S. Chatkaew, R. E. Goldstein, and J. O. Kessler, "Self-concentration and large-scale coherence in bacterial dynamics," Phys. Rev. Lett. **93**, 098103 (2004).
[11]R. Kemkemer, D. Kling, D. Kaufmann, and H. Gruler, "Elastic properties of nematoid arrangements formed by amoeboid cells," Eur. Phys. J. E **1**, 215–225 (2000).
[12]T. Surrey, F. Nédélec, S. Leibler, and E. Karsenti, "Physical properties determining self-organization of motors and microtubules," Science **292**, 1167–1171 (2001).
[13]P. Bendix, G. Koenderink, D. Cuvelier, Z. Dogic, B. Koeleman, W. Brieher, C. Field, L. Mahadevan, and D. Weitz, "A quantitative analysis of contractility in active cytoskeletal protein networks," Biophys. J. **94**, 3126–3136 (2008).
[14]H. Chaté, F. Ginelli, G. Grégoire, and F. Raynaud, "Collective motion of self-propelled particles interacting without cohesion," Phys. Rev. E **77**, 046113 (2008).
[15]I. Buttinoni, J. Bialk'e, F. Kümmel, H. Löwen, C. Bechinger, and T. Speck, "Dynamical clustering and phase separation in suspensions of self-propelled colloidal particles," Phys. Rev. Lett. **110**(23), 238301 (2013).
[16]B. Bhattacherjee, S. Mishra, and S. S. Manna, "Topological-distance-dependent transition in flocks with binary interactions," Phys. Rev. E **92**, 062134 (2015).
[17]S. Pattanayak and S. Mishra, "Collection of polar self-propelled particles with a modified alignment interaction," J. Phys. Commun. **2**, 045007 (2018).
[18]J. P. Singh, S. Kumar, and S. Mishra, "Bond disorder enhances the information transfer in the polar flock," J. Stat. Mech. **2021**, 083217.
[19]V. Narayan, S. Ramaswamy, and N. Menon, "Long-lived giant number fluctuations in a swarming granular nematic," Science **317**, 105–108 (2007).
[20]J. Deseigne, O. Dauchot, and H. Chaté, "Collective motion of vibrated polar disks," Phys. Rev. Lett. **105**, 098001 (2010).
[21]A. R. Sprenger, M. A. Fernandez-Rodriguez, L. Alvarez, L. Isa, R. Wittkowski, and H. Löwen, "Active Brownian motion with orientation-dependent motility: Theory and experiments," Langmuir **36**, 7066–7073 (2020).
[22]X. Zheng, B. ten Hagen, A. Kaiser, M. Wu, H. Cui, Z. Silber-Li, and H. Löwen, "Non-Gaussian statistics for the motion of self-propelled Janus particles: Experiment versus theory," Phys. Rev. E **88**, 032304 (2013).
[23]D. K. Sahu and S. Dhara, "Electric field driven controllable motility of metal-dielectric Janus particles with boojum defects in thin films of a nematic liquid crystal," Phys. Fluids **33**, 087106 (2021).
[24]L. Di Carlo and M. Scandolo, "Evidence of fluctuation-induced first-order phase transition in active matter," arXiv:2202.01010 (2022).
[25]S. Kumar and S. Mishra, "Active nematics with quenched disorder," Phys. Rev. E **102**, 052609 (2020).
[26]J. P. Singh, S. Pattanayak, S. Mishra, and J. Chakrabarti, "Effective single component description of steady state structures of passive particles in an active bath," arXiv:2202.01014 (2022).
[27]S. Malvar and F. R. Cunha, "A theoretical model for studying the nonlinear viscoelastic response of an active fluid undergoing oscillatory shear," Phys. Fluids **33**, 091903 (2021).
[28]A. Dhar, P. S. Burada, and G. P. Raja Sekhar, "Effective medium model for a suspension of active swimmers," Phys. Fluids **33**, 091906 (2021).
[29]C. Lian and W. Zhong, "Active control of transport through nanopores," Phys. Fluids **33**, 071907 (2021).
[30]A. Nagilla, R. Prabhakar, and S. Jadhav, "Linear stability of an active fluid interface," Phys. Fluids **30**, 022109 (2018).
[31]P. Dwivedi, A. Shrivastava, D. Pillai, and R. Mangal, "Rheotaxis of active droplets," Phys. Fluids **33**, 082108 (2021).
[32]A. Daddi-Moussa-Ider, M. Lisicki, H. Löwen, and A. M. Menzel, "Dynamics of a microswimmer-microplatelet composite," Phys. Fluids **32**, 021902 (2020).
[33]P. M. Vinze, A. Choudhary, and S. Pushpavanam, "Motion of an active particle in a linear concentration gradient," Phys. Fluids **33**, 032011 (2021).
[34]S. Sahoo, S. P. Singh, and S. Thakur, "Role of viscoelasticity on the dynamics and aggregation of chemically active sphere-dimers," Phys. Fluids **33**, 017120 (2021).
[35]M. Cavaiola and A. Mazzino, "Self-propelled slender objects can measure flow signals net of self-motion," Phys. Fluids **33**, 053603 (2021).
[36]G. Delhaye, F. Mercier, and V. Teboul, "Simulation of a flat folding nano-swimmer confined in a nanopore," Phys. Fluids **33**, 122001 (2021).
[37]R. Das, M. Kumar, and S. Mishra, "Polar flock in the presence of random quenched rotators," Phys. Rev. E **98**, 060602 (2018).
[38]M. Durve and A. Sayeed, "First-order phase transition in a model of self-propelled particles with variable angular range of interaction," Phys. Rev. E **93**, 052115 (2016).
[39]L. Giomi, T. B. Liverpool, and M. C. Marchetti, "Sheared active fluids: Thickening, thinning, and vanishing viscosity," Phys. Rev. E **81**, 051908 (2010).
[40]S. Ramaswamy, R. A. Simha, and J. Toner, "Active nematics on a substrate: Giant number fluctuations and long-time tails," Europhys. Lett. **62**, 196–202 (2003).
[41]J. P. Singh and S. Mishra, "Phase separation in a binary mixture of self-propelled particles with variable speed," Physica A **544**, 123530 (2020).
[42]V. Semwal, S. Dikshit, and S. Mishra, "Dynamics of a collection of active particles on a two-dimensional periodic undulated surface," Eur. Phys. J. E **44**, 20 (2021).
[43]B. Deußen, Y. Wang, and M. Oberlack, "A deterministic two-phase model for an active suspension with non-spherical active particles using the Eulerian spatial averaging theory," Phys. Fluids **34**, 023302 (2022).
[44]A. Dhar, P. S. Burada, and G. P. R. Sekhar, "Hydrodynamics of active particles confined in a periodically tapered channel," Phys. Fluids **32**, 102005 (2020).
[45]P. Dwivedi, B. R. Si, D. Pillai, and R. Mangal, "Solute induced jittery motion of self-propelled droplets," Phys. Fluids **33**, 022103 (2021).
[46]O. T. Dyer and R. C. Ball, "Influence of thermal fluctuations on active diffusion at large Péclet numbers," Phys. Fluids **33**, 051904 (2021).
[47]M. Rank and A. Voigt, "Active flows on curved surfaces," Phys. Fluids **33**, 072110 (2021).
[48]S. Kumar, J. P. Singh, D. Giri, and S. Mishra, "Effect of polydispersity on the dynamics of active Brownian particles," Phys. Rev. E **104**, 024601 (2021).
[49]S. Dikshit and S. Mishra, "Activity-driven phase separation and ordering kinetics of passive particles," Eur. Phys. J. E **45**, 21 (2022).
[50]F. Peruani, T. Klauss, A. Deutsch, and A. Voss-Boehme, "Traffic jams, gliders, and bands in the quest for collective motion of self-propelled particles," Phys. Rev. Lett. **106**, 128101 (2011).
[51]A. P. Solon and J. Tailleur, "Revisiting the flocking transition using active spins," Phys. Rev. Lett. **111**, 078101 (2013).
[52]A. P. Solon and J. Tailleur, "Flocking with discrete symmetry: The two-dimensional active Ising model," Phys. Rev. E **92**, 042119 (2015).
[53]T. Vicsek, A. Czirók, E. Ben-Jacob, I. Cohen, and O. Shochet, "Novel type of phase transition in a system of self-driven particles," Phys. Rev. Lett. **75**, 1226–1229 (1995).
[54]A. N. Kolmogorov, "Zur Theorie der Markoffschen Ketten," Math. Ann. **112**, 155 (1936).
[55]E. Ising, "Beitrag zur theorie des ferromagnetismus," Z. Phys. **31**, 253–258 (1925).
[56]D. P. Landau and K. Binder, "Frontmatter," in *A Guide to Monte Carlo Simulations in Statistical Physics*, 2nd ed. (Cambridge University Press, 2005), pp. i–iv.
[57]R. Pathria and P. D. Beale, "The canonical ensemble," in *Statistical Mechanics*, 3rd ed., edited by R. Pathria and P. D. Beale (Academic Press, Boston, 2011), pp. 39–90.
[58]S. Mishra, A. Baskaran, and M. C. Marchetti, "Fluctuations and pattern formation in self-propelled particles," Phys. Rev. E **81**, 061916 (2010).
[59]T. R. Malthus, *An Essay on the Principle of Population*, History of Economic Thought Books (McMaster University Archive for the History of Economic Thought, 1798).
[60]E. Bertin, M. Droz, and G. Grégoire, "Boltzmann and hydrodynamic description for self-propelled particles," Phys. Rev. E **74**, 022101 (2006).

[61]R. Das, M. Kumar, and S. Mishra, "Order-disorder transition in active nematic: A lattice model study," Sci. Rep. **7**, 7080 (2017).
[62]D. Forster, D. R. Nelson, and M. J. Stephen, "Large-distance and long-time properties of a randomly stirred fluid," Phys. Rev. A **16**, 732–749 (1977).
[63]P. M. Chaikin, T. C. Lubensky, and T. A. Witten, *Principles of Condensed Matter Physics* (Cambridge University Press, Cambridge, 1995), Vol. 10.
[64]K. Binder, E. Luijten, M. Müller, N. B. Wilding, and H. W. J. Blöte, "Monte Carlo investigations of phase transitions: Status and perspectives," Physica A **281**, 112–128 (2000).
[65]K. Binder, "Applications of the Monte Carlo method in statistical physics," *Applications of the Monte Carlo Method in Statistical Physics*, Topics in Current Physics (Springer, 1987).